Journal of *Marine Science and Engineering*

MDPI

Article

Vertical Bearing Capacity for Pile-Ring Composite Foundations in Clay

Jianfeng Zhou [1], Weisen Cai [1], Jian Yu [2,*] and Zhaoyun Xiao [1]

[1] College of Civil Engineering, Huaqiao University, Xiamen 361021, China; zhoujf0912@hqu.edu.cn (J.Z.); 23013086001@stu.hqu.edu.cn (W.C.); zyxiao@hqu.edu.cn (Z.X.)
[2] Department of Geotechnical Engineering, Tongji University, Shanghai 200092, China
* Correspondence: 002yujian@tongji.edu.cn

Abstract

Evaluating the vertical bearing capacity of offshore wind turbine pile-ring composite foundations under complex marine environmental loads is critical for ensuring engineering safety. This study employs the rigorously validated T-EMSD upper-bound method to conduct a three-dimensional numerical analysis of the vertical bearing capacity of pile-ring composite foundations in saturated clay. It systematically investigates the influence of soil homogeneity (η, diameter ratio (D/B), embedment ratio (L/B), and external shaft friction coefficient (α) on the bearing capacity factor N_c, and reveals the associated failure mechanism through velocity field analysis. The results indicate that the bearing capacity factor N_c increases significantly with the diameter ratio D/B. The system exhibits optimal bearing performance when the pile shaft friction is fully mobilized (α = 1) in homogeneous soil ($\eta = 1$). Moreover, as the embedment ratio L/B increases, the plastic zone extends downward along the pile shaft, enhancing the deep foundation effect. Based on parametric analysis, a predictive formula for the net bearing capacity factor of the pile-ring composite foundation under homogeneous conditions is established. Verified against existing numerical methods and experimental data, the formula demonstrates an error margin within $\pm$5%, indicating its good suitability for engineering applications. Furthermore, by establishing a ratio relationship, the net bearing capacity factor under heterogeneous conditions is correlated with that under homogeneous conditions. This enables a more in-depth analysis of the influences of soil strength heterogeneity and external shaft friction coefficient on the vertical bearing capacity of the pile-ring composite foundation. The work presented in this paper provides a theoretical basis for the design and bearing capacity assessment of this type of composite foundation.

Keywords: pile-ring composite foundation; T-EMSD; nonhomogeneous clay; ultimate bearing capacity

Check for updates

Academic Editor: Jianhong Ye

Received: 24 January 2026
Revised: 28 February 2026
Accepted: 28 February 2026
Published: 4 March 2026

Copyright: © 2026 by the authors. Licensee MDPI, Basel, Switzerland. This article is an open access article distributed under the terms and conditions of the Creative Commons Attribution (CC BY) license.

1. Introduction

Against the backdrop of intensifying global energy crises and growing ecological and environmental concerns, the development and utilization of renewable energy have become a crucial pathway for nations to achieve their "dual carbon" goals and ensure energy security. Offshore wind power, with its distinct advantages of abundant and stable wind resources, no occupation of land space, and high power generation efficiency, has emerged as a significant growth area in the renewable energy sector. In recent years, offshore wind farms have been deployed in deeper and more remote waters. However,

the harsh marine environmental conditions in these areas—characterized by strong winds, huge waves, and complex geological settings—impose stringent demands on the bearing capacity, stability, and cost-effectiveness of the supporting foundation structures. The foundation, which serves as the core load-bearing component of an offshore wind turbine structure, directly determines the safe operation and service life of the turbine. Given that foundation engineering accounts for 25% to 35% of the total project investment, the development of efficient and reliable foundation types is therefore pivotal for advancing the offshore wind industry into deeper waters.

In current deep-water offshore wind projects, traditional monopile foundations, despite their widespread application, face significant limitations under complex loading conditions: On the one hand, the lateral stiffness and lateral bearing capacity of a monopile are constrained by its diameter and embedment depth. Cyclic horizontal loads induced by strong winds and huge waves can easily lead to excessive deformation and even cumulative damage to the pile, making it difficult to meet the long-term safety requirements for operation in deep waters [1]. On the other hand, improving the vertical bearing capacity of a monopile relies on increasing its diameter or embedment depth, which not only escalates the difficulties in pile fabrication and transportation but also leads to a non-linear increase in construction costs. Meanwhile, isolated ring foundations (e.g., spread footings), while capable of enhancing the vertical bearing capacity by enlarging the base area, possess relatively weak lateral stiffness. They are susceptible to overturning failure under combined horizontal loads and bending moments, especially in soft clay strata, where the problem of differential settlement is prominent, rendering them unsuitable for complex load scenarios in deep waters. Therefore, enhancing the bearing performance of offshore wind foundations is crucial for the stability of offshore wind turbine structures.

To ensure offshore wind turbine foundations possess excellent load-bearing performance, numerous scholars have proposed various novel composite foundation types and conducted extensive research on their bearing characteristics. A series of findings has been obtained through experimental testing and numerical simulations, confirming their technical advantages. Regarding lateral bearing performance, Stone et al. verified through physical model tests that adding a bearing plate around a monopile foundation can simultaneously enhance its lateral stiffness and ultimate bearing capacity, clarifying that the lateral capacity is provided by a combination of the pile's lateral resistance and plate-soil interface friction [2]. Haiderali and Madabhushi proposed a composite improvement scheme involving the addition of a skirt to a monopile foundation in submarine clay, significantly enhancing its lateral capacity by strengthening passive earth pressure [3]. Trojnar, based on field tests and three-dimensional finite element analysis, further validated the lateral stiffness advantage of composite foundations in clay environments [4]. Focusing on bending resistance and collaborative load-bearing characteristics, Lehane et al. discovered through centrifuge model tests that the platform structure can efficiently transfer superstructure bending moments, substantially strengthening the overall bending resistance of the foundation [5]. Anastasopoulos and Theofilou used three-dimensional finite element simulations to reveal the dynamic response patterns of pile-ring foundations under environmental and seismic loads, confirming the synergistic gain in the bending moment capacity [6]. Wang et al. proposed a monopile-platform composite scheme. Validation through combined centrifuge tests and numerical simulations confirmed its stability under complex loading [7]. Concerning vertical bearing capacity and comprehensive performance, Sun Yanguo et al. conducted a comparative analysis using ABAQUS software, revealing that the vertical bearing capacity of pile-platform foundations increases exponentially with platform diameter, while that of pile-barrel foundations is dominated by the barrel's embedment depth [8]. Yang et al. and Li et al. innovatively developed an umbrella-shaped composite foundation

and investigated its bearing-capacity evolution and anti-scour performance through a series of tests [9,10]. El-Marassi systematically revealed the failure envelope characteristics of composite foundations under combined loading through centrifuge model tests and numerical simulations [11]. The aforementioned research, addressing different load types such as lateral, bending, and vertical, all confirms the significant advantages of composite foundations. However, research on the vertical bearing capacity of pile-ring composite foundations in saturated clay remains limited. The systematic understanding of the influence patterns and underlying mechanisms of key parameters of the ring structure—such as soil homogeneity (η), diameter ratio (D/B), embedment ratio (L/B), and external shaft friction coefficient (α)—on vertical bearing performance is insufficient, making it difficult to provide direct and precise theoretical support for engineering design.

To further clarify the novelty and engineering contribution of this work, it should be emphasized that the pile–ring composite foundation exhibits a coupled failure mechanism and load-transfer mode that cannot be obtained by directly superposing existing isolated pile or ring-footing theories. In particular, this study (i) establishes a unified three-dimensional upper-bound framework for pile–ring foundations; (ii) systematically quantifies the coupled effects of D/B, L/B, η, and α on N_c and identifies the transition of failure mechanisms; and (iii) proposes a closed-form predictive model with explicitly stated applicability ranges for practical use. Notably, the present analyses were conducted under short-term undrained Tresca conditions, and therefore provide upper-bound estimates for monotonic vertical loading. For offshore wind foundations subjected to long-term consolidation or cyclic loading, changes in s_u, interface conditions, and accumulated deformation may alter the absolute values of N_c; however, the parametric trends and mechanism interpretations remain useful as first-order guidance.

This study employs the T-EMSD method [12] to conduct a systematic three-dimensional numerical analysis of the vertical bearing capacity of pile-ring composite foundations in saturated clay. T-EMSD is an upper-bound limit analysis method developed from the EMSD method [13]. It focuses on obtaining the load-displacement upper-bound solution for plane-strain problems through iterative computations. Unlike conventional limit analysis methods that solve for the upper-bound bearing capacity by constructing a plastic deformation field, T-EMSD transforms the energy conservation equation into an equivalent elastic virtual work equation through mathematical manipulation. The equivalent elastic analysis is then directly used to compute the upper-bound solution for the plastic problem. This approach avoids the complexity of the incremental loading process inherent in traditional limit analyses, allowing for the direct calculation of the vertical upper-bound resistance under a prescribed total displacement. The key to T-EMSD lies in converting the soil's strain-strength relationship into a strain-dependent equivalent non-linear shear modulus. This replaces the optimization-solving process in EMSD, enabling the acquisition of the load-displacement curve through elastic iterations. When the applied displacement is sufficiently large, the vertical resistance calculated by T-EMSD can approach the upper-bound value of the ultimate load. Compared to the complexity of constructing a continuous velocity field required by traditional methods, T-EMSD significantly enhances computational efficiency and applicability under complex conditions. It has been successfully applied to foundation bearing capacity calculations [14] and three-dimensional tunnel face stability analyses [15], providing an efficient and reliable solution for assessing the bearing capacity of complex soil-structure interactions.

The obtained upper-bound solutions are presented in terms of the bearing capacity factor N_c. The rationality of the T-EMSD method is verified by comparing its results, obtained from models degenerated to a ring foundation and a pile foundation, with those from the existing literature. Subsequently, a parametric analysis is conducted to systematically

summarize the vertical bearing behavior of the pile-ring composite foundation. A further in-depth analysis is performed to investigate the influences of the diameter ratio of the pile-ring foundation, soil strength heterogeneity, embedment ratio of the pipe pile, and external shaft friction coefficient on the uplift bearing capacity of the pile-ring composite foundation. This research provides a scientific basis for elucidating the vertical bearing mechanism of pile-ring composite foundations and improving their design theory. It also lays a theoretical foundation for the rational assessment of the bearing capacity of such foundations in practical engineering.

2. Problem Description

This study investigates the vertical bearing capacity of pile-ring composite foundations in saturated clay. The problem definition is illustrated in Figure 1. The subject of study is a composite foundation formed by combining a circular cross-section pile with an embedment depth L and diameter B, and a ring foundation with an outer diameter D (and an inner diameter equal to B). It operates under vertical loading in a saturated clay environment. The saturated clay is approximated as a Tresca material. Assuming the soil unit weight is γ, the undrained shear strength $s_{u(z)}$ varies linearly with depth z as follows:

$$s_{u(z)} = s_{u0} + \rho z \tag{1}$$

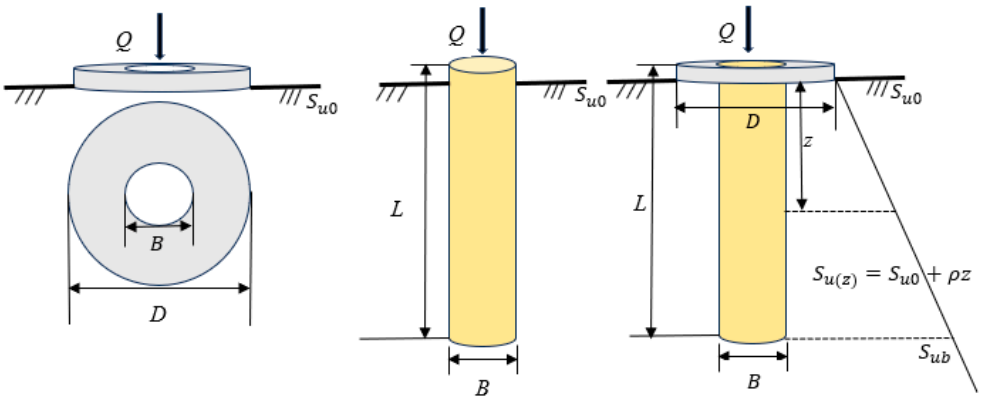


Figure 1. Schematic of the ring, closed-ended pile, and pile-ring composite foundations.

In the equation, s_{u0} is the undrained shear strength of the clay at the ground surface, and ρ is the slope of the undrained shear strength profile. This linear variation model reasonably reflects the non-uniformity of strength in the depth direction of nonhomogeneous clay. To further quantify the non-uniformity of soil strength, a normalized strength non-uniformity coefficient is defined, with the soil strength non-uniformity expressed using the normalized coefficient η:

$$\eta = \frac{s_{u0}}{s_{ub}} = \frac{s_{u0}}{s_{u0} + \rho L} \tag{2}$$

In the equation, s_{ub} is the undrained shear strength of the clay at the pile base depth. When η is 1, it corresponds to a homogeneous soil. To facilitate the comparative analysis of the results, the obtained ultimate bearing capacity of the foundation is made dimensionless using the geometric dimensions and the shear strength of the saturated clay. The normalized uplift bearing capacity factor N_c is defined as the ratio of the vertical bearing capacity per unit area of the pile cross-section to the soil strength:

$$N_c = \frac{4Q}{\pi B^2 s_{u0}} \tag{3}$$

In the equation, Q is the vertical ultimate bearing capacity, and B is the pile diameter. The definition of this normalized parameter is analogous to that of the bearing capacity factor for shallow foundations. It effectively characterizes the relationship between the vertical bearing performance of the pile-ring composite foundation and the soil's mechanical parameters, facilitating comparative analysis under different working conditions. This study employs a heterogeneous clay model to investigate the influence of clay strength heterogeneity and geometric parameters of the pile-ring composite foundation on its vertical bearing performance. The findings provide theoretical support for design under complex conditions in practical engineering.

3. Method of Analysis

Osman and Bolton (2004, 2005) [16] proposed a Mobilizable Strength Design (MSD) method. It can effectively describe the load-displacement relationship in the analysis of soil response. Subsequently, Klar and Osman (2008) [13] refined the MSD method and proposed an Extended Mobilizable Strength Design (EMSD) method. EMSD introduces the concept of fictitious load steps, allowing the deformation field to evolve dynamically during the loading process. This enables the calculation of a more precise load-displacement curve. However, EMSD requires the accumulation of strain increments for each fictitious load step and necessitates optimization of the deformation field at each step, which makes the implementation process complex and computationally demanding.

To address this, Huang et al. (2015) [17] constructed a continuous deformation field using multilayer elastic mechanics displacement solutions and proposed the Total-displacement Fictitious Loading Upper Bound Limit Analysis (T-EMSD) theory. Through theoretical derivation, they obtained an iterative control equation for determining the elastic parameters of each layer via elastic iterative computation. This section will expound on the theoretical formulation of the T-EMSD method under three-dimensional conditions and its numerical implementation. The implementation involves the secondary development of the commercial finite element analysis software ABAQUS 6.14 to investigate the bearing capacity of pile-ring composite foundations in undrained saturated clay.

In upper-bound limit analysis, undrained clay that satisfies the incompressibility condition and any imposed velocity boundary conditions is typically assumed to be a Tresca material. For the Tresca yield criterion, Shield and Drucker proved that the upper bound theorem can be expressed as:

$$\begin{array}{c} \int_S T_i v_i dS + \int_V f_i v_i dV \le \int_V 2 s_u \left|\dot{\varepsilon}_{max}\right| dV + \int_A s_u |\Delta v_i| dA \\ = \int_S T_i^* u_i dS + \int_V f_i u_i dV \quad (i = 1, 2, 3) \end{array} \tag{4}$$

In the equation: T_i and f_i are the surface traction and body force vectors acting on boundaries S and V, respectively; v_i is the admissible velocity field; s_u is the undrained shear strength of the soil; $\left|\dot{\varepsilon}_{max}\right|$ is the maximum principal strain of the plastic strain field compatible with the admissible velocity field v_i; Δv_i is the relative velocity change amplitude on the soil discontinuity surface A; T_i^* is the upper bound load determined by the plastic upper bound theorem.

For a continuous velocity field, Equation (4) can be expressed as the energy conservation formula for internal and external work increments using the EMSD method proposed by Klar and Osman (2008) [13], as shown in Equation (5):

$$\int_V 2 c_m(\varepsilon_s) \delta\varepsilon_{max} dV = \int_S T_i^* \delta u_i dS + \int_V f_i \delta u_i dV \quad (i = 1, 2, 3) \tag{5}$$

In the equation: $c_m(\varepsilon_s)$ is the soil strength corresponding to ε_s; engineering shear strain $\varepsilon_s = \varepsilon_1 - \varepsilon_3$; absolute maximum principal strain increment $\delta\varepsilon_{max} = \max(|\delta\varepsilon_1|, |\delta\varepsilon_2|, |\delta\varepsilon_3|)$;

δu_i is the compatible incremental displacement field. The ideal elastoplastic stress-strain relationship can be expressed as

$$c_m(\varepsilon_S) = min[G_s\varepsilon_S\ , s_u] \tag{6}$$

where G_s is the soil shear modulus, and the maximum value of c_m is s_u.

If only the first loading step is considered, that is, $\varepsilon_{ij} = \delta\varepsilon_{ij}$, and substituting Equation (6) into Equation (5) yields:

$$\int_V 2min[G\varepsilon_S\ , s_u]\delta\varepsilon_s\delta\varepsilon_{max}dV = \int_S T_i^*\delta u_i dS + \int_V f_i\delta u_i dV\ \ (i = 1,2,3) \tag{7}$$

Considering that under undrained conditions $\delta\varepsilon_1 + \delta\varepsilon_2 + \delta\varepsilon_3 = 0$, the discussion of strain order only exists in two cases: ① $\varepsilon_1 \geq \delta\varepsilon_2 \geq 0 \geq \delta\varepsilon_3$ and ② $\delta\varepsilon_1 \geq 0 \geq \delta\varepsilon_2 \geq \delta\varepsilon_3$. For case ① $\delta\varepsilon_1 \geq \delta\varepsilon_2 \geq 0 \geq \delta\varepsilon_3$, Equation (7) can be rewritten in the following form:

$$\begin{array}{l} \int_V 2\eta_1 min\left[G_s\ , \frac{s_u}{|\delta\varepsilon_1 - \delta\varepsilon_3|}\right]|\delta\varepsilon_1^2 + \delta\varepsilon_2^2 + \delta\varepsilon_3^2|dV \\ = \int_S T_i^*\delta u_i dS + \int_V f_i\delta u_i dV \qquad (i = 1,2,3) \end{array} \tag{8}$$

In the equation: $\eta_1 = \frac{\delta\varepsilon_1^2 - \delta\varepsilon_1\delta\varepsilon_3}{\delta\varepsilon_1^2 + \delta\varepsilon_2^2 + \delta\varepsilon_3^2}$ is a function of soil strain state. According to the undrained condition, the soil strain state function η_1 can be equivalently expressed as $\eta_1 = \frac{1 - \delta\varepsilon_3/\delta\varepsilon_1}{2\left(1 + \delta\varepsilon_3/\delta\varepsilon_1 + \left(\delta\varepsilon_3/\delta\varepsilon_1\right)^2\right)}$. By defining $\eta_1 min\left[G_s\ , \frac{s_u}{|\delta\varepsilon_1 - \delta\varepsilon_3|}\right]$ as the equivalent elastic shear modulus $\widetilde{G}$, Equation (5) can be expressed as:

$$\int_V 2\widetilde{G}\delta\varepsilon_{ij}\delta\varepsilon_{ij}dV = \int_S T_i^*\delta u_i dS + \int_V f_i\delta u_i dV \qquad (i = 1,2,3) \tag{9}$$

Equation (9) is, in form, a typical elastic virtual work equation. The concept of an elastic modulus does not exist in plastic limit analysis. However, in the Total-displacement Fictitious Loading Upper Bound Limit Analysis (T-EMSD) method derived from the aforementioned mathematical transformation, an equivalent shear modulus $\widetilde{G}$ exists at each loading step. As shown in Figure 2, in the ABAQUS implementation, Equation (9) is solved by iteratively updating the strain-dependent equivalent shear modulus $\widetilde{G}$ for all soil elements. In this study, the L2 norm of the normalized vertical displacement error is adopted as the convergence criterion, with the maximum allowable error threshold defined as Max Allowable Difference (taken as 0.15, dimensionless). Convergence is declared when, during the iteration process, the overall normalized vertical displacement error at key foundation nodes is $\leq$0.15 and the relative change in the total reaction force between two consecutive iterations falls below 1×10^{-3}. Huang et al. (2015) [17] have proven that if the displacement δu_i applied in a single step is sufficiently large, the final bearing capacity obtained from this elastic problem constitutes an upper-bound solution to the original problem. Since $\widetilde{G}$ depends on the current strain level and is not a constant value, Equation (9) must be solved through elastic iterative computation.

The T-EMSD method is formulated based on the fundamental principles of upper-bound analysis. By incorporating the derivation of stress-strain relationships, it transforms the upper-bound problem of limit analysis into an equivalent elastic problem for the solution. As shown in Figure 3, this approach enables T-EMSD to directly compute the upper-bound reaction force RF_i under a prescribed total displacement u_i through iterative calculation, rather than optimization. The iterative calculation for a given total displacement begins with the corresponding elastic solution. The upper-bound reaction force is then approximated by repeatedly performing an elastic analysis and updating the equivalent

shear modulus. When a relatively large total displacement u_j is applied, T-EMSD can also directly compute the corresponding upper-bound reaction force RF_j without an incremental loading process. This method employs an elastic displacement field to approximate the plastic deformation field and assigns an equivalent strain-dependent shear modulus to each soil element. This treatment eliminates the need to pre-construct a velocity field, allowing T-EMSD to obtain the load-displacement upper-bound solution through iterative calculation, similar to solving an elastic problem, rather than through optimization. One application of this method is to obtain the upper-bound load-displacement curve by connecting each independently calculated reaction force. The second method involves attaining the upper-bound load by directly applying a sufficiently large displacement. T-EMSD has been validated in the analysis of two-dimensional plane-strain problems and the ultimate bearing capacity of strip foundations on slopes. It is capable of directly calculating the upper-bound reaction force under a given displacement without requiring an incremental loading process. Studies by Li et al. (2019) [18] indicate that the soil stiffness index G/s_u has little influence on the ultimate load determined by T-EMSD, but it affects the development of the load-displacement curve. A larger G/s_u value results in a smaller displacement at which the upper-bound load is reached. Therefore, a consistent stiffness index (e.g., 10,000) is typically adopted for T-EMSD analyses. To further confirm this assumption, a brief sensitivity check was conducted by repeating representative cases with alternative stiffness indices (G/s_u = 5000 and 20,000), and the resulting ultimate N_c changed only marginally; therefore, the conclusions reported herein are insensitive to the adopted stiffness index.

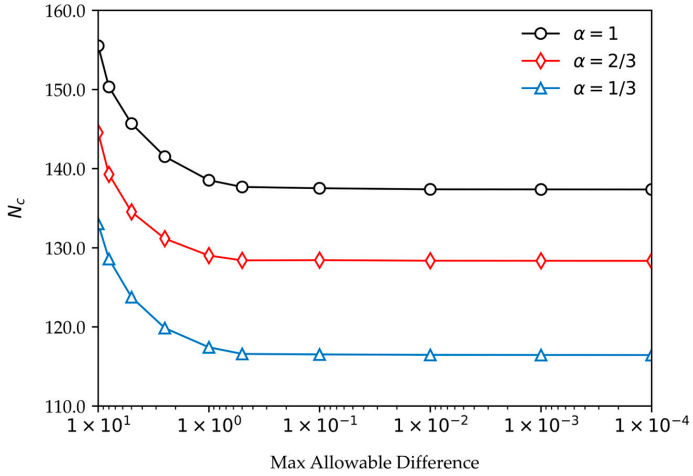


Figure 2. The effect of Max Allowable Difference on N_c.

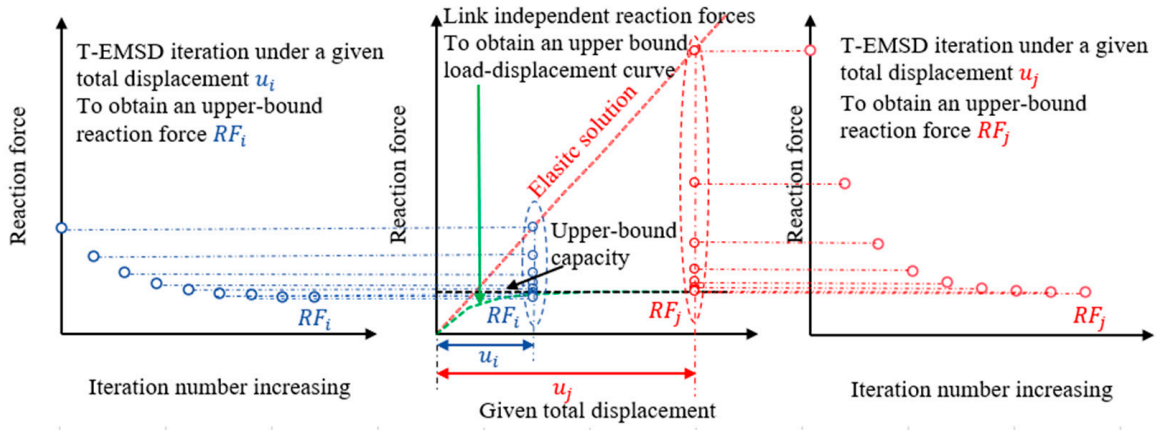


Figure 3. Features of the T-EMSD method.

4. Results and Analysis of the Pile-Ring Composite Foundation

4.1. Results and Analysis

This study treats the upper-bound bearing capacity problem of the pile-ring composite foundation in saturated clay as an axisymmetric problem. A quarter-model was employed to perform elastic finite element analysis using the ABAQUS software. Figure 4 shows the mesh schematic for the case with $L/B = 8$ and $D/B = 4$. A fine mesh is used near the pile-ring composite foundation, while a coarse mesh is applied in regions farther away, ensuring computational accuracy at a reasonable computational cost. Figure 5 presents a representative mesh-refinement check, which confirms that further mesh refinement near the foundation results in a negligible change in the ultimate N_c.

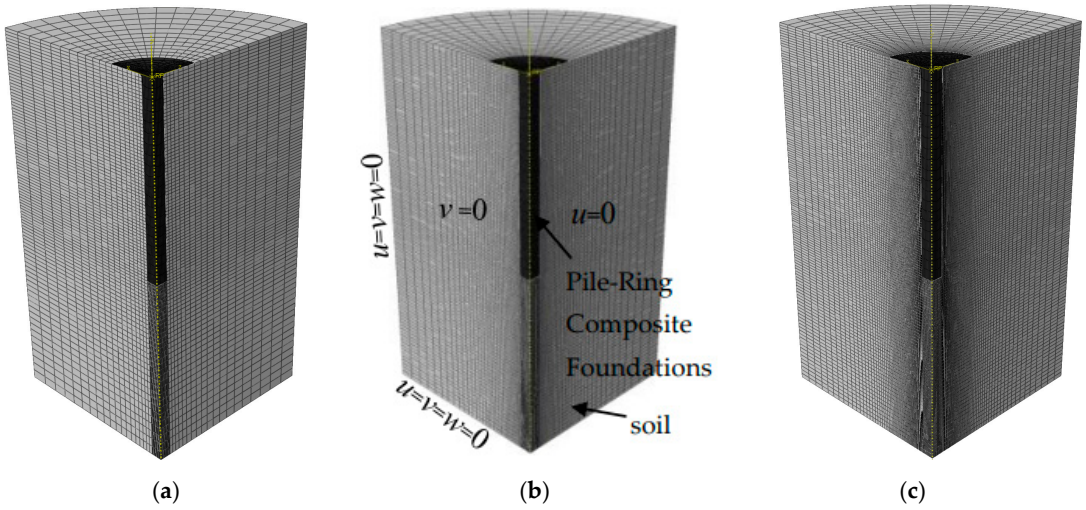


Figure 4. Schematic of the mesh for a pile-ring composite foundation with $L/B = 8$ and $D/B = 4$: (**a**) 38,706 elements, (**b**) 82,459 elements, and (**c**) 121,045 elements.

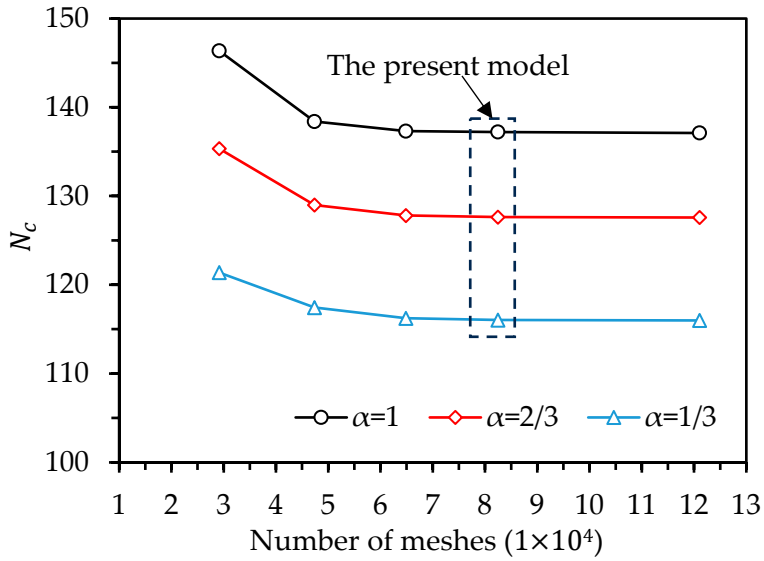


Figure 5. Sensitivity of mesh refinement in the vicinity of pile-ring composite foundation.

In this model, the pile-ring composite foundation is simulated as a rigid material, and the soil is modeled as an elastic material. The undrained shear strength is $s_{u0} = 20$ kPa, and the elastic modulus is $E = 20{,}000 s_{u0}$. To simulate undrained conditions, the Poisson's ratio v was theoretically set to 0.5. However, in the actual implementation using the ABAQUS script, a value of $v = 0.495$ was adopted to avoid singularity of the stiffness matrix. To satisfy

the continuity requirement, displacement boundaries on all faces were fixed in all directions, except for the ground surface (modeled as a free surface) and the symmetry plane, where only normal displacement is allowed. This ensures that the frictional energy dissipation at the boundaries is not neglected, thereby guaranteeing that the corresponding T-EMSD solution is a strict upper bound. To mitigate the influence of model boundary effects on the finite element calculation results, a series of preliminary analyses was conducted to determine an adequate spatial domain. The final dimensions of the soil mass were set to a height of $2L$ and a diameter of $16D$.

Figure 6a presents the bearing capacity factor for the pile-ring composite foundation with $L/B = 0$. This case is equivalent to a ring foundation ($D > B$). The figure illustrates the variation of the ultimate bearing capacity factor with the diameter ratio D/B for a ring foundation under pure vertical loading in homogeneous soil ($\eta = 1.0$). A comparison is made among results derived from four distinct numerical approaches: the T-EMSD upper-bound method (this study); the small-strain finite element analysis of Lee et al. (2016) [19]; the finite element limit analysis of Wang et al. (2022) [20]; and the three-dimensional finite difference analysis of Hamlaoui et al. (2022) [21]. It can be observed that the bearing capacity factor increases significantly with an increase in D/B. The curve derived from the present method shows good agreement with the results of Lee et al. (2016) [19], Wang et al. (2022) [20], and Hamlaoui et al. (2022) [21] across the entire D/B range. Quantitatively, the relative differences at the common D/B values reported in these studies range from -2.14% to $+5.06\%$ (Table 1), which is considered acceptable given the differences in numerical implementations and boundary settings. This indicates that the proposed T-EMSD method is consistent with other methods under homogeneous soil conditions, verifying the reliability of this model for analyzing the bearing capacity of pile-ring composite foundations.

Figure 6b–f systematically investigates the characteristics of the vertical ultimate bearing capacity factor for the pile-ring composite foundation in homogeneous soil. The analysis covers a range of embedment ratios L/B (4, 8, 12, 16, and 20). The results show that the ultimate bearing capacity factor of the pile-ring composite foundation system increases significantly with an increase in the diameter ratio D/B. When $D/B = 1$, the structure degenerates into a solid single pile with a diameter of B, whose bearing capacity is primarily provided by shaft friction and end resistance. For this case, the results calculated by the present method show excellent agreement with the upper-bound solution data points from Yu et al. (2023) [22], further confirming the reliability of the model for pile-ring composite foundation analysis. As D/B increases, the load-bearing contribution of the ring foundation becomes more pronounced, forming a composite load-bearing system of the pile and the ring foundation. Consequently, the vertical ultimate bearing capacity factor of the pile-ring composite foundation exhibits exponential growth. Meanwhile, the external shaft friction coefficient α has a certain influence on the vertical ultimate bearing capacity of the pile-ring composite foundation; the bearing capacity factor N_c decreases as α decreases. As L/B increases, the deep foundation effect of the pile is enhanced, leading to an overall increase in the bearing capacity factor. By analyzing the numerical results in Figure 6, a predictive formula for the net bearing capacity factor N_c of the pile-ring foundation can be derived based on the predictive formula for the net bearing capacity factor of the ring foundation (Appendix A) and that of the pile foundation (Appendix B).

$$N_c = \frac{4Q}{S_{u0}\pi B^2} = N_c^r\left(\frac{D^2}{B^2} - 1\right) + N_c^p \tag{10}$$

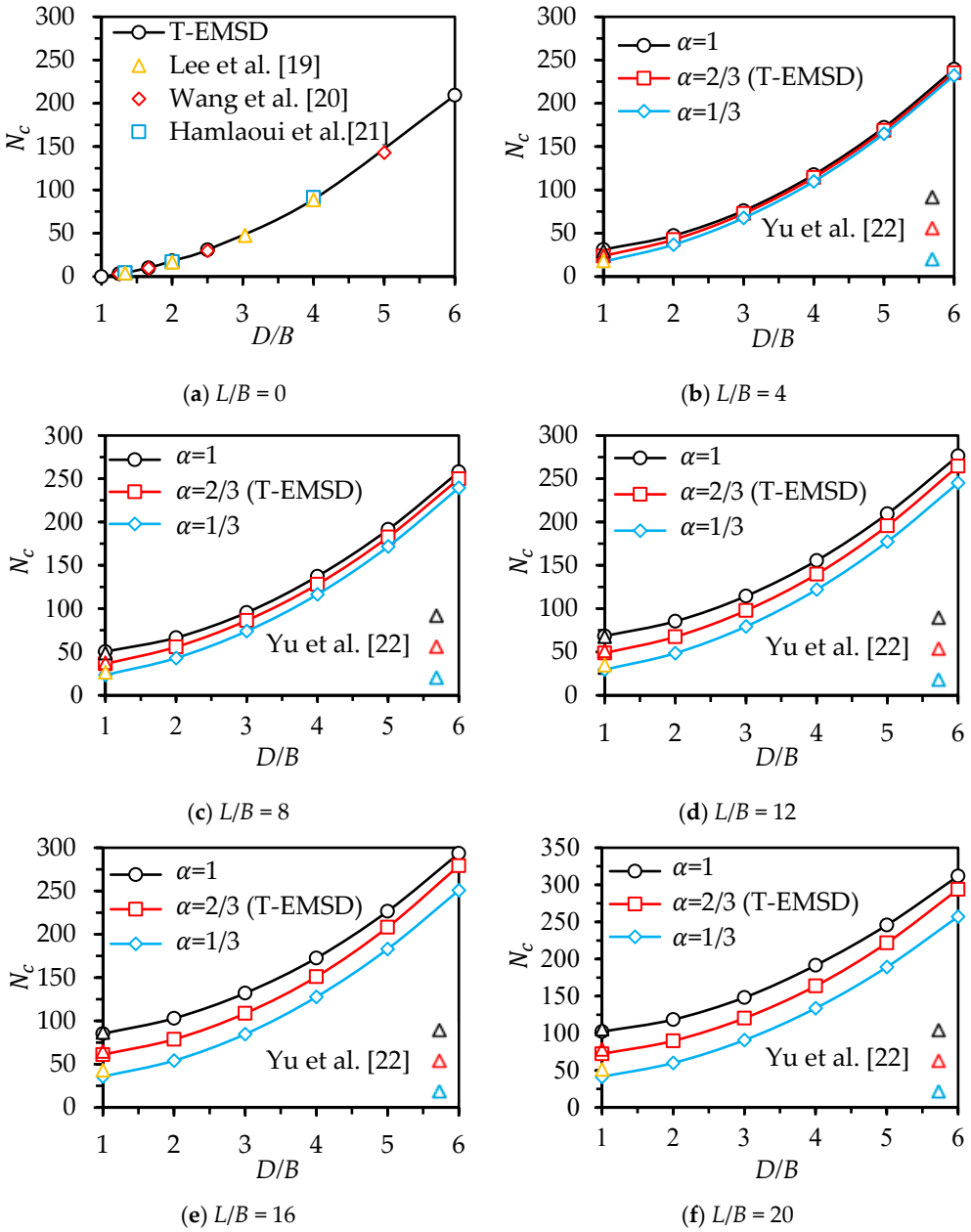


Figure 6. Bearing capacity factor for the pile-ring composite foundation.

Table 1. Quantitative comparison of N_c for ring foundation case ($L/B = 0$) at common D/B values.

Reference	D/B	N_c (T-EMSD)	N_c (Ref)	Rel. Diff (%)
Lee et al. (2016) [19]	2.00	17.52	16.83	+4.10
Lee et al. (2016) [19]	4.00	89.25	88.80	+0.51
Wang et al. (2022) [20]	1.25	3.12	2.98	+4.70
Wang et al. (2022) [20]	1.67	10.18	9.69	+5.06
Wang et al. (2022) [20]	2.50	30.91	29.82	+3.66
Hamlaoui et al. (2022) [21]	2.00	17.52	17.19	+1.96
Hamlaoui et al. (2022) [21]	4.00	89.25	91.20	−2.14

Figure 7 indicates that as the ratio of ring diameter to pile diameter (D/B) increases, the spatial influence range of the velocity field expands significantly. The plastic zone develops from the vicinity of the pile shaft to the extensive shallow soil surrounding the

ring, demonstrating that enlarging the ring size can effectively mobilize a larger volume of soil, thereby enhancing the overall uplift bearing capacity. Figure 8 presents the velocity field distributions for different values of α. When $\alpha = 1$, the velocity field is fully developed around the pile and beneath the ring foundation, indicating that the soil mass enters a fully plastic state and the pile shaft friction is fully mobilized. When α decreases to 2/3, the extent of the velocity field contracts in the middle and lower parts of the pile. When $\alpha = 1/3$, the velocity field becomes further concentrated near the ring foundation, and the participation of the soil adjacent to the pile shaft is significantly reduced. This evolution intuitively reveals the controlling effect of α on the system's failure mode: full mobilization of the pile shaft friction can effectively engage the resistance of deeper soil layers, thereby improving the overall bearing capacity. Figure 9 shows the velocity field distributions corresponding to the pile-ring composite foundation for different embedment ratios (L/B). As L/B increases, the velocity field gradually extends towards the lower part of the pile shaft and into deeper soil layers. The plastic zone notably propagates downward along the pile, reflecting the progressive enhancement of the pile's deep bearing mechanism. This evolution indicates that with an increasing embedment ratio, the pile shaft friction is more fully mobilized, and the volume of soil participating in load-bearing expands. Consequently, the overall stability and bearing capacity of the composite foundation are effectively enhanced.

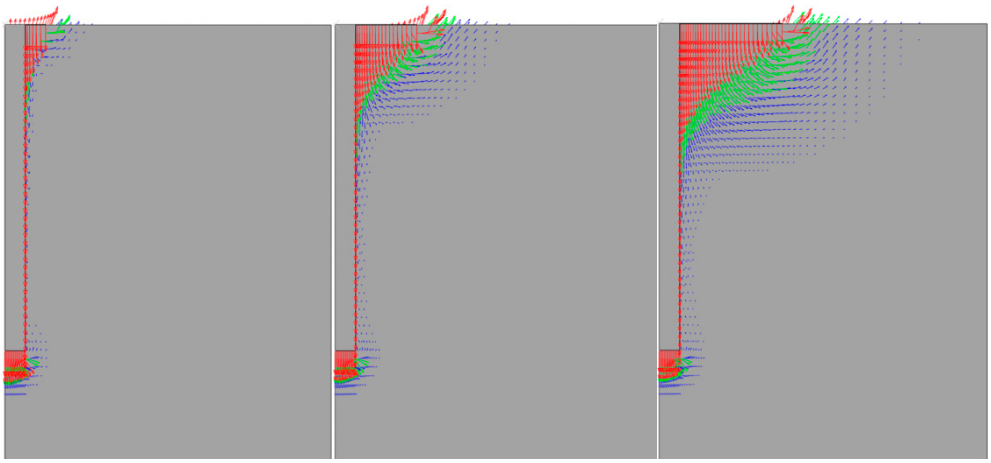


Figure 7. Velocity contours for the pile-ring composite foundation with different D/B ratios ($\eta = 1.0$).

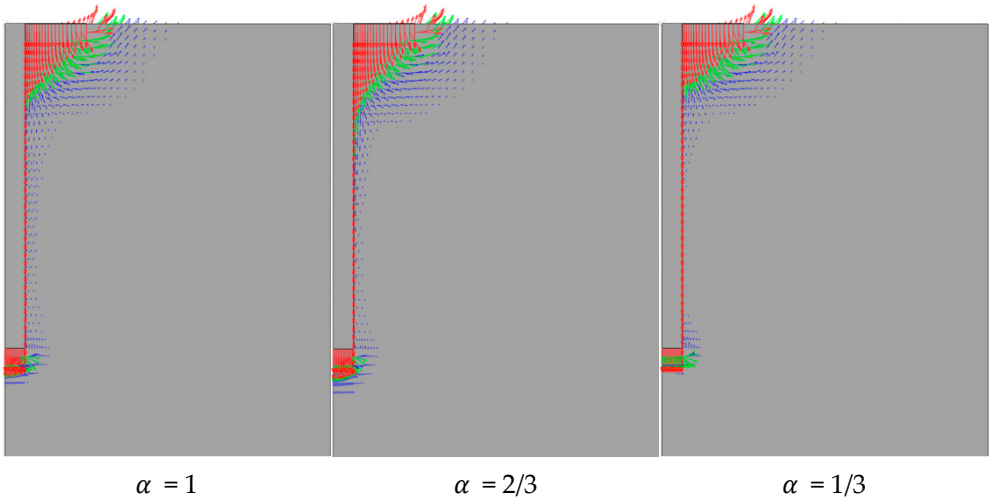


Figure 8. Velocity contours for the pile-ring composite foundation with different external shaft roughness coefficients (α).

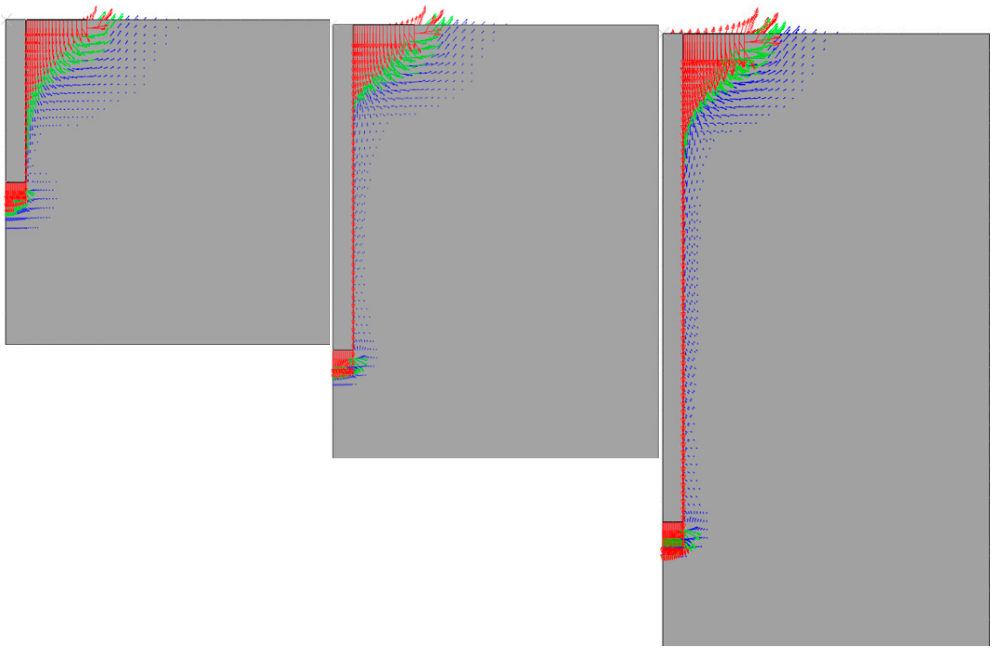
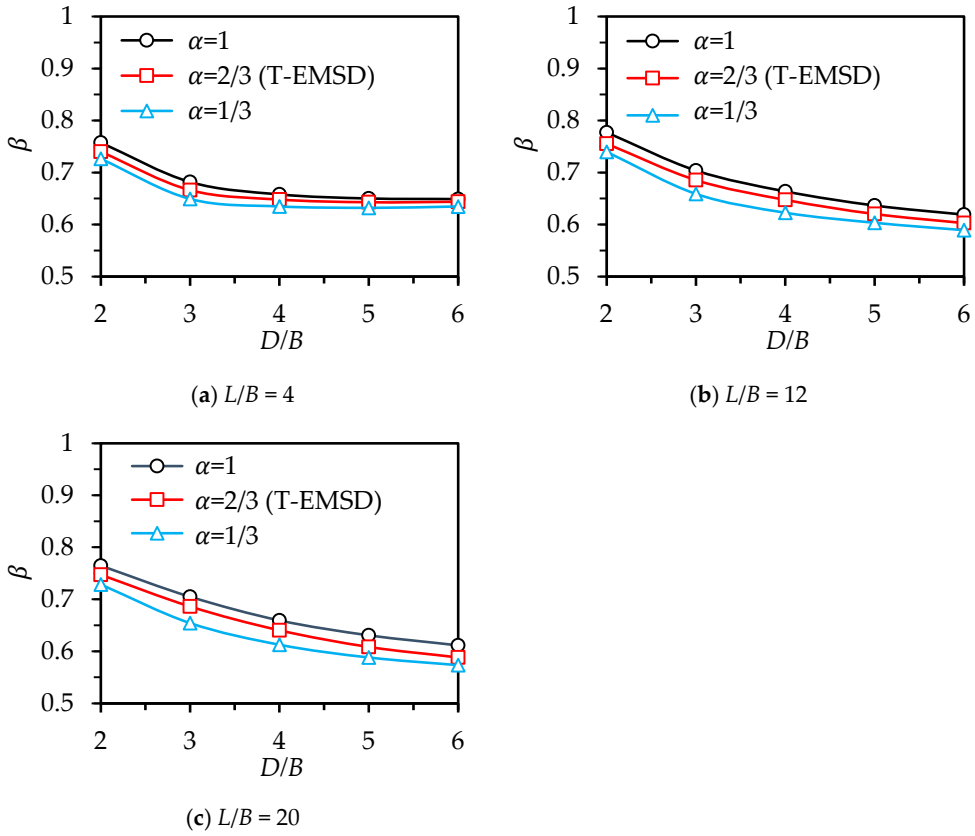


Figure 9. Velocity contours for the pile-ring composite foundation with different embedment ratios (L/B).

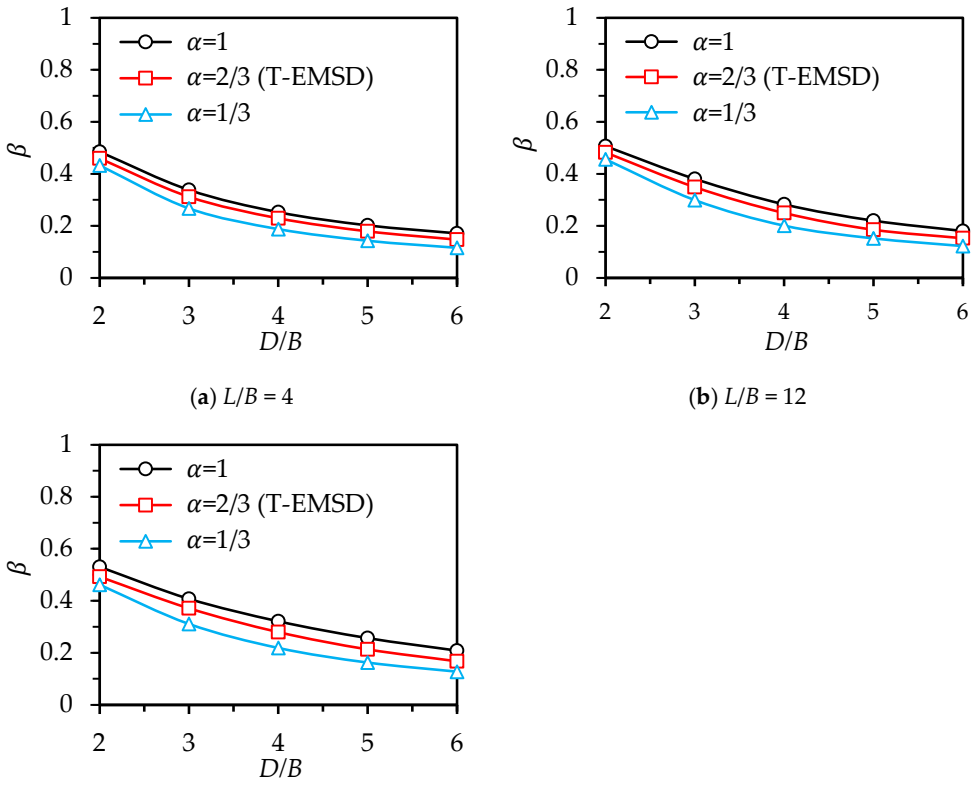
The ratio of the net bearing capacity factor of the pile-ring foundation in heterogeneous soil to that in homogeneous soil is defined as β. Figures 10 and 11 illustrate the variation of the ratio (β) of the bearing capacity factor of the pile-ring composite foundation in heterogeneous soils ($\eta = 0.5$ and $\eta = 0.0$) to its counterpart in homogeneous soil, with respect to the diameter ratio D/B. The analysis indicates that the bearing capacity ratio is less than 1 for both cases and shows a decreasing trend as D/B increases. This demonstrates that soil heterogeneity significantly reduces the net bearing capacity of the pile-ring composite foundation. Furthermore, compared to the case with $\eta = 0.5$, the case with $\eta = 0.0$ (zero strength at the ground surface) exhibits an overall lower ratio and a more pronounced decline, indicating that a stronger degree of heterogeneity leads to a more severe reduction in bearing capacity. In conjunction with the velocity contour plot in Figure 12, it is shown that as the heterogeneity coefficient η decreases, soil flow becomes more prone to occur in the weaker upper soil layers, resulting in a decline in the overall bearing capacity. As seen from Figure 13 ($\eta = 0.5$), when D/B increases, although the ring foundation's influence zone expands, it primarily remains within the relatively low-strength shallow soil. Deeper and higher-strength soil layers are not effectively mobilized. This explains why merely enlarging the ring size (increasing D/B) in heterogeneous soil leads to a reduction in bearing capacity relative to the homogeneous case ($\eta = 1.0$). This is because the increased ring area enhances the reliance on the weak, shallow soil, failing to establish an effective cooperative load-bearing mechanism with the deeper soil strata. In terms of stress transfer, a larger D/B increases the proportion of load carried by the annular ring area, which mainly mobilizes near-surface bearing resistance; when $\eta < 1$, this shallow zone is weaker and yields earlier, so the additional ring area does not translate into proportional capacity gain. Conversely, the inner pile can mobilize deeper, stronger soil through shaft friction and base resistance; therefore, configurations with moderate D/B and sufficient L/B promote a more effective shallow–deep cooperative mechanism in heterogeneous clay.



(**a**) $L/B = 4$ (**b**) $L/B = 12$

(**c**) $L/B = 20$

Figure 10. Ratio of bearing capacity factor (heterogeneous, $\eta = 0.5$ to homogeneous) versus D/B.



(**a**) $L/B = 4$ (**b**) $L/B = 12$

(**c**) $L/B = 20$

Figure 11. Ratio of bearing capacity factor (heterogeneous, $\eta = 0$ to homogeneous) versus D/B.

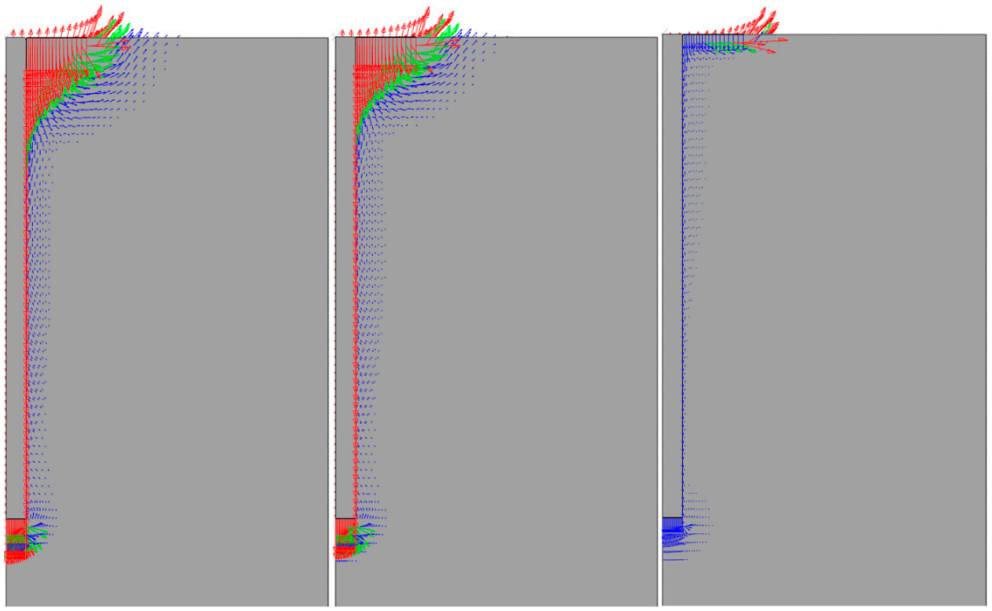


Figure 12. Velocity contours for the pile-ring composite foundation for different heterogeneity coefficients (η).

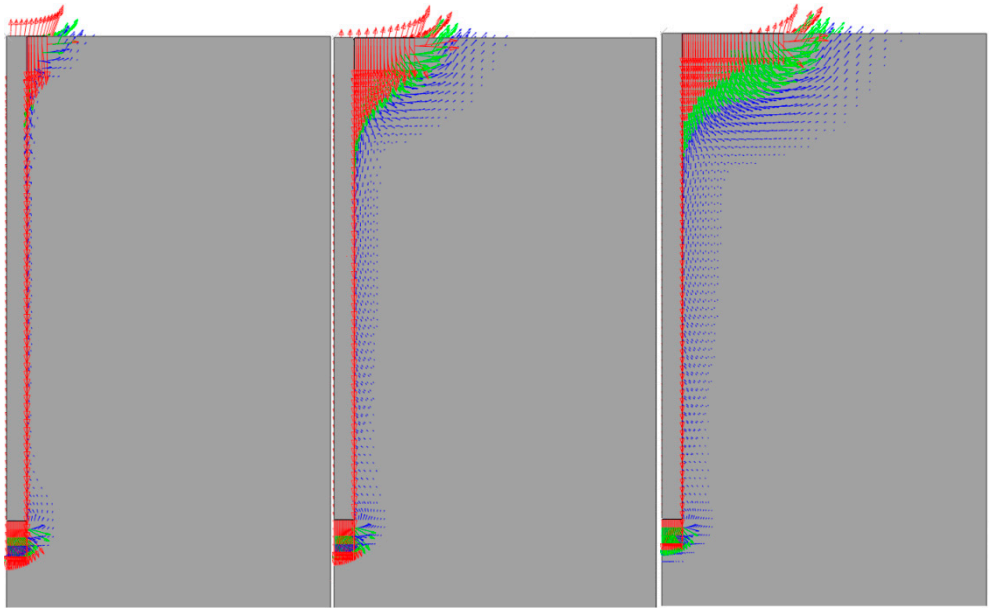


Figure 13. Velocity contours for the pile-ring composite foundation for different D/B ratios ($\eta = 0.5$).

4.2. Verification of Bearing Capacity Formula

To interpret Equation (10) under pile–ring coupling, this study defines an interaction index ψ and a residual term ΔN_c: $\psi = N_c/(N_c^r + N_c^p)$ and $\Delta N_c = N_c - (N_c^r + N_c^p)$, where N_c is obtained from Figure 6b–f, N_c^r is obtained from the degenerated ring case ($L/B = 0$; Figure 6a), and N_c^p is read from the degenerated pile case at $D/B = 1$ (Figure 6b–f).

Plastic zones beneath the ring and around the pile may overlap, which would reduce the net resistance compared with a direct sum of the two degenerated systems ($\psi < 1$ or $\Delta N_c < 0$). Conversely, the pile occupies the space inside the ring and transfers a portion of the load to deeper soil, and this mechanism increases the net resistance compared with the direct sum ($\psi > 1$ or $\Delta N_c > 0$). The numerical results show that the two effects have

comparable magnitudes within the investigated ranges; consequently, ψ remains close to unity.

For the homogeneous cases shown in Figure 6, ψ ranges from 0.957 to 1.043 within the investigated ranges ($4 \leq L/B \leq 20$, $2 \leq D/B \leq 6$, $0 \leq \alpha \leq 1$). Representative values are listed in Table 2.

Table 2. Representative interaction index ψ and residual ΔN_c (η = 1.0).

L/B	α	D/B	N_c (num)	N_c^r (L/B = 0)	N_c^p (D/B = 1)	ψ	ΔN_c
4	1	2	47.370	18.228	31.290	0.957	−2.148
4	2/3	2	42.620	18.228	23.844	1.013	0.549
4	1/3	2	36.790	18.228	17.244	1.037	1.318
12	1	4	155.597	89.250	68.365	0.987	−2.017
12	2/3	4	139.855	89.250	48.689	1.014	1.917
12	1/3	4	122.126	89.250	29.652	1.027	3.224
20	1	6	311.915	209.417	102.223	1.001	0.275
20	2/3	6	293.909	209.417	72.335	1.043	12.157
20	1/3	6	257.267	209.417	41.463	1.025	6.388

The predictive formula for the net bearing capacity factor of the pile-ring foundation is verified against the numerical results. It is noted that direct laboratory/field data for pile–ring composite foundations remain limited; therefore, the present validation focuses on the numerical database, while degenerated ring/pile cases are benchmarked against published numerical and experimental results. The results presented in Figure 14 show that the predictions from the proposed formula generally exhibit an error of within 5% when compared to the numerical results. Overall, the proposed predictive formula demonstrates high accuracy and reliability, making it suitable for practical engineering applications.

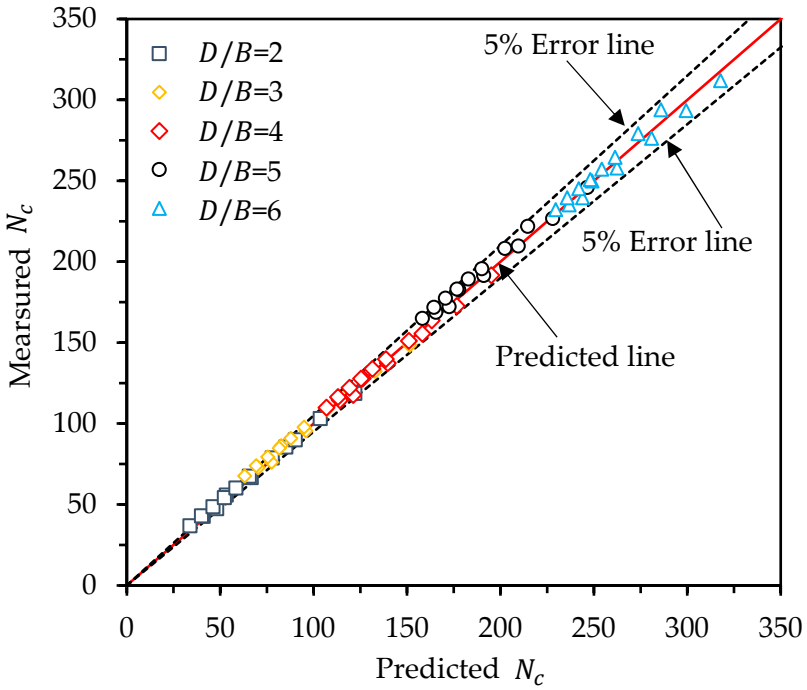


Figure 14. Comparison between the predicted and numerical results for the net bearing capacity coefficient N_c of the pile-ring foundation.

5. Conclusions

This study employed the numerical upper-bound method (T-EMSD) to analyze the ultimate vertical bearing capacity of uplift pile-ring composite foundations in saturated clay and derived an upper-bound solution for the vertical bearing capacity. The validity of the adopted method was verified by comparing it with the results from the existing literature. The specific conclusions are as follows:

(1) The bearing capacity factor N_c increases with the diameter ratio D/B and embedment ratio L/B, and it is strongly controlled by the pile–soil interface condition. When the external shaft friction coefficient $\alpha = 1$, shaft friction is fully mobilized and N_c reaches its maximum. When α decreases, the shaft contribution is reduced, and the failure mechanism becomes shallower. Based on the parametric database, a predictive formula for the net bearing capacity factor was established for homogeneous clay ($\eta = 1.0$) and shows good agreement with the numerical results and available reference data within $0 \leq D/B \leq 6$, $4 \leq L/B \leq 20$, and $0 \leq \alpha \leq 1$, with most errors within approximately $\pm 5\%$; extrapolation beyond these ranges should be treated with caution.

(2) Soil strength heterogeneity ($\eta < 1.0$) reduces the bearing capacity, and the reduction becomes more pronounced as η decreases. In heterogeneous clay, increasing D/B alone tends to rely more on the weaker near-surface soil and may yield diminishing or even adverse gains; therefore, adopting a moderate D/B together with a sufficiently large L/B is recommended to mobilize deeper, stronger soil layers and develop a more effective shallow–deep cooperative mechanism. Direct experimental validation of pile–ring composite foundations remains limited; future centrifuge/large-scale model tests and field monitoring are recommended to further verify the coupled mechanism and extend its applicability.

Author Contributions: Methodology, W.C.; Resources, Z.X.; Writing—original draft, J.Z.; Writing—review & editing, J.Y. All authors have read and agreed to the published version of the manuscript.

Funding: This work was supported by the National Key R&D Program of China (Grant No. 2024YFB2605500).

Data Availability Statement: Data will be made available upon request.

Conflicts of Interest: The authors declare no conflict of interest.

Appendix A. Bearing Capacity Formula for the Ring Foundation

Results and Verification of the Formula

Figure A1 illustrates the evolution of the normalized net bearing capacity coefficient N_c^r for the ring foundation with respect to D/B under homogeneous conditions. To provide a convenient predictive formula for the bearing capacity of the ring foundation, an analysis was conducted based on the computational results of the parametric analysis shown in Figure 13. The fitted predictive formula for the net bearing capacity coefficient is as follows:

$$N_c^r = (6 - 0.4\frac{1}{A}) \tag{A1}$$

In this equation, $A = D/B$.

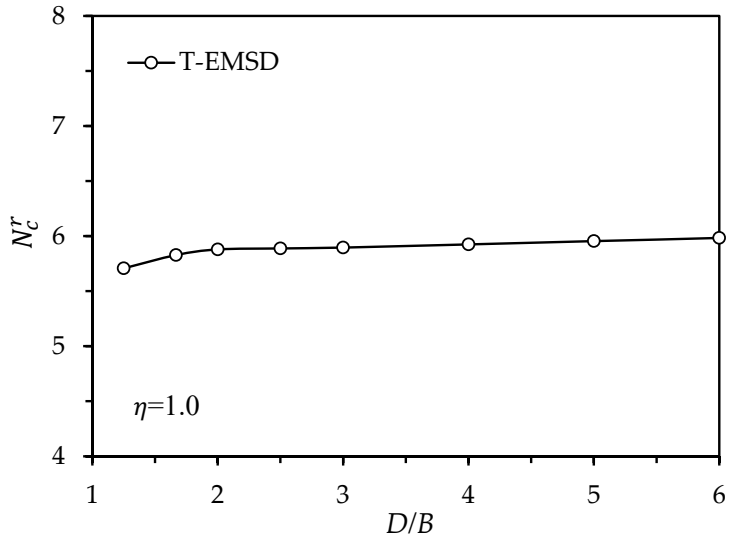


Figure A1. Bearing capacity factor of the ring foundation.

Figure A2 compares the predictions of the proposed formula for the net bearing capacity coefficient N_c^r of the ring foundation with the numerical results obtained from four different methods: T-EMSD, Lee et al. (2016) [19], Kedar et al. (2021) [23], Wang et al. (2016) [20], and Hamlaoui et al. (2022) [21]. In the figure, the horizontal axis represents the predicted values from the formula, and the vertical axis represents the numerical results from the respective methods. The analysis indicates that the vast majority of the data points are closely distributed around the line of perfect agreement and mostly fall within the error margin, verifying the high accuracy of the predictive formula. Among these, the predictions from the T-EMSD method used in this paper align well with the ideal line. The numerical solutions obtained using the other methods also show a similar distribution trend, demonstrating good consistency. This result further confirms the reliability of the proposed predictive model for evaluating the net bearing capacity coefficient of ring foundations on homogeneous soil conditions.

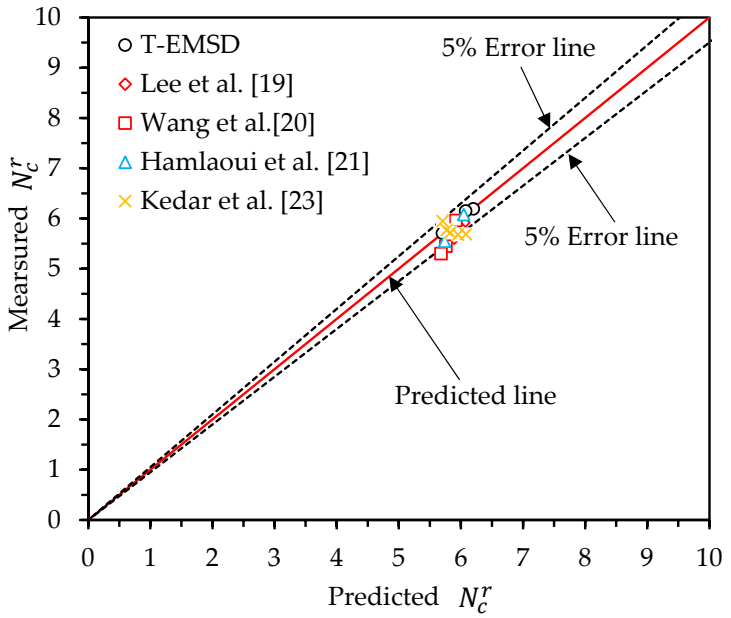


Figure A2. Comparison and validation of the predictive formula for the net bearing capacity coefficient of the ring foundation.

Appendix B. Bearing Capacity Formula for the Closed-Ended Pile

Results and Verification of the Formula

Figure A3 presents the evolution of the normalized net bearing capacity coefficient for a closed-ended pile with respect to the embedment ratio and the external shaft roughness coefficient. The research indicates that the vertical net bearing capacity of a closed-ended pile comprises contributions from both shaft friction and end-bearing resistance, which exhibit distinctly different mechanical response mechanisms. The shaft contribution component shows a linear positive correlation with the embedment ratio (L/B), while the end-bearing component demonstrates nonlinear characteristics. When $L/B \leq 20$, the end-bearing component increases gradually with the pile's embedment ratio. For $L/B > 20$, influenced by the deep foundation effect, the end-bearing component gradually approaches a stable value. Based on nonlinear regression analysis, a predictive formula for the net bearing capacity of closed-ended piles was established, which accounts for the superposition effect of individual contributions. This formula explicitly characterizes the coupling relationship between the linear shaft term and the asymptotic end-bearing term, providing a more accurate theoretical predictive model for engineering applications.

$$N_c^p\left(\frac{L}{B},\alpha\right) = 4\alpha\frac{L}{B} + \begin{cases} \alpha\left(0.62\frac{L}{B}+3\right)+9 & \frac{L}{B} < 20 \\ 15.4\alpha + 9 & \frac{L}{B} \geq 20 \end{cases} \quad \text{(A2)}$$

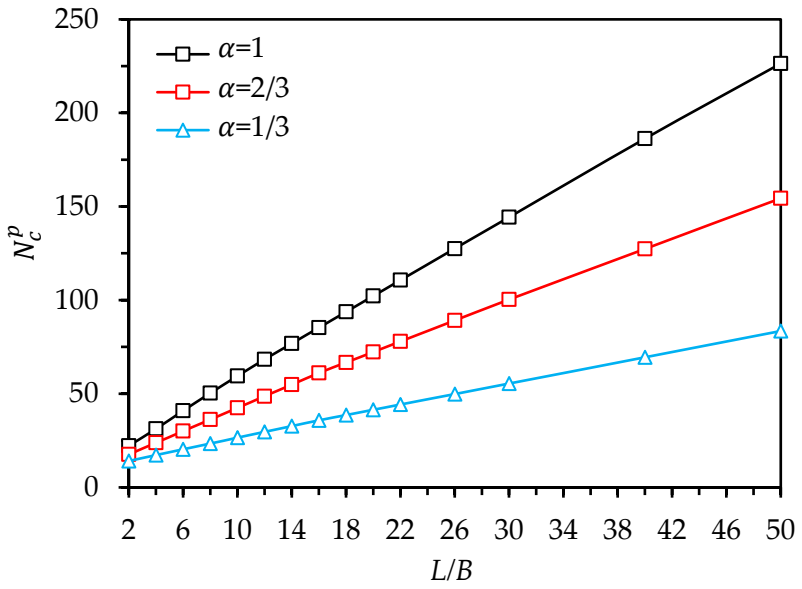


Figure A3. Relationship between the net bearing capacity coefficient N_c^p of the closed-ended pile and the embedment ratio (L/B).

Figure A4 compares the predictions of the proposed formula for the net bearing capacity coefficient of closed-ended piles with the laboratory test results from Azim (1985) [24] and the upper-bound solutions from Yu et al. (2023) [22]. The results demonstrate that the predictions from the proposed formula are generally 9.2% higher than the measured ultimate bearing capacities. The maximum discrepancy with existing upper-bound solutions in the literature does not exceed 7.1%, and the predictions show a distribution close to the measured values. Overall, the proposed predictive formula exhibits high accuracy and reliability, making it suitable for practical engineering applications.

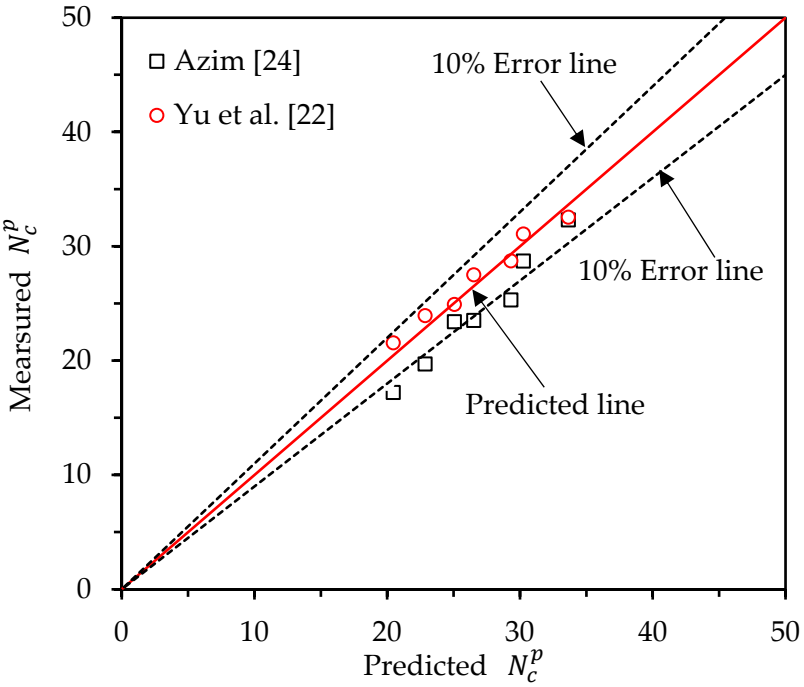


Figure A4. Comparison and validation of the predictive formula for the net bearing capacity coefficient of the closed-ended pile.

References

1. Wengang, Q.; Fuping, G. Effects of scour on horizontal bearing behavior of monopile foundations for offshore wind turbines. *Sci. Sin. Phys. Mech. Astron.* **2016**, *46*, 10. [CrossRef]
2. Stone, K.; Arshi, H.S.; Zdravkovic, L. Use of a bearing plate to enhance the lateral capacity of monopiles in sand. *J. Geotech. Geoenviron. Eng.* **2018**, *144*, 4018051.
3. Haiderali, A.; Madabhushi, G. Improving the lateral capacity of monopiles in submarine clay. *Proc. Inst. Civ. Eng.-Ground Improv.* **2016**, *169*, 239–252.
4. Trojnar, K. Lateral stiffness of hybrid foundations: Field investigations and 3D FEM analysis. *Géotechnique* **2013**, *63*, 355–367. [CrossRef]
5. Lehane, B.M.; Pedram, B.; Doherty, J.A.; Powrie, W. Improved performance of monopiles when combined with footings for tower foundations in sand. *J. Geotech. Geoenviron. Eng.* **2014**, *140*, 4014027. [CrossRef]
6. Anastasopoulos, I.; Theofilou, M. Hybrid foundation for offshore wind turbines: Environmental and seismic loading. *Soil Dyn. Earthq. Eng.* **2016**, *80*, 192–209. [CrossRef]
7. Wang, X.; Zeng, X.; Yang, X.; Li, J. Feasibility study of offshore wind turbines with hybrid monopile foundation based on centrifuge modeling. *Appl. Energy* **2018**, *209*, 127–139. [CrossRef]
8. Sun, Y.G.; Xu, C.S.; Du, X.L.; Wang, P.G.; Xi, R.Q.; Sun, Y.L. Comparison of the bearing capacities of composite foundations for offshore wind turbines. *Chin. J. Eng.* **2022**, *44*, 1098–1107.
9. Yang, Q.; Yu, P.; Liu, Y.; Liu, H.; Zhang, P.; Wang, Q. Scour characteristics of an offshore umbrella suction anchor foundation under the combined actions of waves and currents. *Ocean Eng.* **2020**, *202*, 106701. [CrossRef]
10. Li, H.; Liu, H.; Liu, S. Dynamic analysis of umbrella suction anchor foundation embedded in seabed for offshore wind turbines. *Geomech. Energy Environ.* **2017**, *10*, 12–20.
11. El-Marassi, M. *Investigation of Hybrid Monopile-Footing Foundation Systems Subjected to Combined Loading*; The University of Western Ontario: London, ON, Canada, 2011.
12. Yu, J.; Huang, M.; Li, S.; Leung, C.F. Load-displacement and upper-bound solutions of a loaded laterally pile in clay based on a total-displacement-loading EMSD method. *Comput. Geotech.* **2017**, *83*, 64–76. [CrossRef]
13. Klar, A.; Osman, A.S. Load–displacement solutions for piles and shallow foundations based on deformation fields and energy conservation. *Géotechnique* **2008**, *58*, 581–589. [CrossRef]
14. Li, S.; Yu, J.; Huang, M.; Leung, C.F. Upper bound analysis of rectangular surface footings on clay with linearly increasing strength. *Comput. Geotech.* **2021**, *129*, 103896. [CrossRef]
15. Huang, M.; Li, S.; Yu, J.; Tan, J.Q.W. Continuous field based upper bound analysis for three-dimensional tunnel face stability in undrained clay. *Comput. Geotech.* **2018**, *94*, 207–213. [CrossRef]

16. Osman, A.; Bolton, M. A new design method for retaining walls in clay. *Can. Geotech. J.* **2004**, *41*, 451–466. [CrossRef]
17. Huang, M.S.; Yu, J.; Zhang, C.R. *p–y* curves of laterally loaded piles in clay based on strain path approach. *Chin. J. Geotech. Eng.* **2015**, *10*.
18. Li, S.; Huang, M.; Yu, J. Continuous field based upper-bound analysis for the undrained bearing capacity of strip footings resting near clay slopes with linearly increased strength. *Comput. Geotech.* **2019**, *105*, 168–182. [CrossRef]
19. Lee, J.K.; Jeong, S.; Lee, S. Undrained bearing capacity factors for ring footings in heterogeneous soil. *Comput. Geotech.* **2016**, *75*, 103–111. [CrossRef]
20. Wang, A.; Zhang, Y.; Xia, F.; Luo, R.; Wang, N. Ultimate Bearing Capacity of Ring Foundations Embedded in Undrained Homogeneous Clay. *Geofluids* **2022**, *2022*, 6382799. [CrossRef]
21. Hamlaoui, S.; Messameh, A.; Mabrouki, A.; Bougouffa, I.; Bouaicha, A. Three-dimensional elasto-plastic analysis for the undrained capacity of ring and circular footings embedded in heterogeneous clay. *Transp. Infrastruct. Geotechnol.* **2023**, *10*, 856–870.
22. Zhu, K.W.; Yu, J.; Huang, M.S. Upper bound analysis of uplift piles in saturated clay and soil plug effect. *Rock Soil Mech.* **2023**, *44*, 1995–2004.
23. Birid, K.; Choudhury, D. Undrained bearing capacity factor Nc for ring foundations in cohesive soil. *Int. J. Geomech.* **2021**, *21*, 6020038. [CrossRef]
24. Azim, M.F. *Ultimate Uplift Capacity of Group Piles in Clay*; ProQuest Dissertations & Theses: Ann Arbor, MI, USA, 1985.

Disclaimer/Publisher's Note: The statements, opinions and data contained in all publications are solely those of the individual author(s) and contributor(s) and not of MDPI and/or the editor(s). MDPI and/or the editor(s) disclaim responsibility for any injury to people or property resulting from any ideas, methods, instructions or products referred to in the content.